J. Ocean Univ. China (Oceanic and Coastal Sea Research)
DOI 10.1007/s11802-017-3069-2
ISSN 1672-5182, 2017 16 (2): 223-232
http://www.ouc.edu.cn/xbywb/
E-mail:xbywb@ouc.edu.cn

Numerical Simulation of Bubble Plumes and an Analysis of Their Seismic Attributes

LI Canping[1)], GOU Limin[2), *], and YOU Jiachun[3)]

1) *Laboratory of Ocean Remote Sensing and Information Technology*, *Guangdong Ocean University*, *Zhanjiang* 524088, *P. R. China*
2) *School of Ocean Sciences*, *China University of Geosciences (Beijing)*, *Beijing* 100083, *P. R. China*
3) *School of Geophysics and Information Technology*, *China University of Geosciences (Beijing)*, *Beijing* 100083, *P. R. China*

(Received November 24, 2015; revised December 1, 2016; accepted December 23, 2016)

Abstract To study the bubble plume's seismic response characteristics, the model of a plume water body has been built in this article using the bubble-contained medium acoustic velocity model and the stochastic medium theory based on an analysis of both the acoustic characteristics of a bubble-contained water body and the actual features of a plume. The finite difference method is used for forward modelling, and the single-shot seismic record exhibits the characteristics of a scattered wave field generated by a plume. A meaningful conclusion is obtained by extracting seismic attributes from the pre-stack shot gather record of a plume. The values of the amplitude-related seismic attributes increase greatly as the bubble content goes up, and changes in bubble radius will not cause seismic attributes to change, which is primarily observed because the bubble content has a strong impact on the plume's acoustic velocity, while the bubble radius has a weak impact on the acoustic velocity. The above conclusion provides a theoretical reference for identifying hydrate plumes using seismic methods and contributes to further study on hydrate decomposition and migration, as well as on distribution of the methane bubble in seawater.

Key words plume; seismic attributes; natural gas hydrate; scattered wave; numerical simulation

1 Introduction

China suffers from a severe energy shortage. Natural gas hydrates have become an attractive alternative energy source to governments and scientific circles around the globe due to their shallow reservoir depth, widespread distribution, high availability and high energy density (Zhang *et al.*, 2013). Survey research in recent years indicates that the South China Sea is a highly important hydrate resource prospect. In addition to the acquisition of hydrate samples, a large number of geological evidence (mud diapirs, pockmarks, authigenic carbonates and seep fauna) related to seep activity have been observed (Huang *et al.*, 2005; Huang *et al.*, 2008). Consequently, large-scale studies have been carried out to predict or confirm the possible existence of hydrates in the Xisha trough, the Dongsha slope, the southwest slope in Taiwan, the Nansha trough and Okinawa troughs in China (Zhang *et al.*, 2013).

A seafloor cold seep refers to a marine geological phenomena wherein the gas or fluid from the submarine sedimentary strata (or deeper) is rejected into the sea by means of gushing or seepage, which is another new research field of marine geology following modern seafloor hot spring activity (Di *et al.*, 2008; Luan *et al.*, 2010). A large amount of gas gushing from a cold seep into the seawater can form a bubble plume. As the mark of seafloor hydrate occurrence and an important means by which hydrates decompose and release methane, seafloor cold seep activity and the accompanied methane seepage not only contribute to the complex marine biogeochemical cycle and ecological process but also occupy a significant position in the research on the global carbon cycle and associated climate effects. Therefore, research on the characteristics of methane seepage related to cold seep activity is particularly important (Chen *et al.*, 2006; Ye *et al.*, 2011).

It is estimated that there are over 900 seafloor cold seep activity areas active in the global marine environment (Di *et al.*, 2010). Bush Hill in the northern Gulf of Mexico is a typical example of the development of cold seep activity (Tryon and Brown, 2004) simultaneous with the production of natural gas hydrate (Macdonalda *et al.*, 2005). The ocean bottom of Hydrate Ridge in Cascadia is also an area of cold seep, with the extensive development of natural gas hydrate (Tryon *et al.*, 2002). Multiple cold

* Corresponding author. Tel: 0086-10-82322162
E-mail: goulm@163.com

seeps and plumes have been detected by side scan sonar in the Hikurangi marginal sea adjacent to the North Island of New Zealand (Klaucke *et al.*, 2010). Cold seep and methane plume have been found at the edge of the Niger Delta as well (Bayon *et al.*, 2011). Chen and his research group (Chen *et al.*, 2004; Chen and Cathles, 2005; Chen *et al.*, 2007; Feng *et al.*, 2009a, 2009b; Tong and Chen, 2012) have obtained notable results since they began engaging in research concerning seafloor cold seep fluid deposits (natural gas hydrate and cold seep carbonate) in 1998. Seven major offshore cold seep areas (points) were initially confirmed, including six areas distributed in the South China Sea and one in the East China Sea (Luan *et al.*, 2010). Multiple bubble plumes have since been found worldwide, such as at the bottom of the west rim of the Barents Sea (Sauter *et al.*, 2006), the continental margin of the Hydrate Ridge in Cascadia (Shipboard Scientific Party, 2002), the Okhotsk Sea (Fig.1) (Luan *et al.*, 2010), the Gulf of Mexico (Sassen *et al.*, 2001), the UT-04 ridge in the Naoetsu Basin at the convergent margin of the sea of Japan (Gong *et al.*, 2006), and other sea areas (Freire *et al.*, 2011) including mud volcanos in the Mediterranean (Charloua *et al.*, 2003), which are rich in hydrates. These plume bubbles carry hydrate erupting from beneath the ocean bottom, forming the seafloor phenomenon of 'flame' reaching heights of up to 1300 m as observed in the Black Sea (Greinert *et al.*, 2006). Large quantities of plume bubbles can be observed at the volcanic vent of the Santa Barbara Channel in California, as shown in Fig.2 (Leifer, 2010).

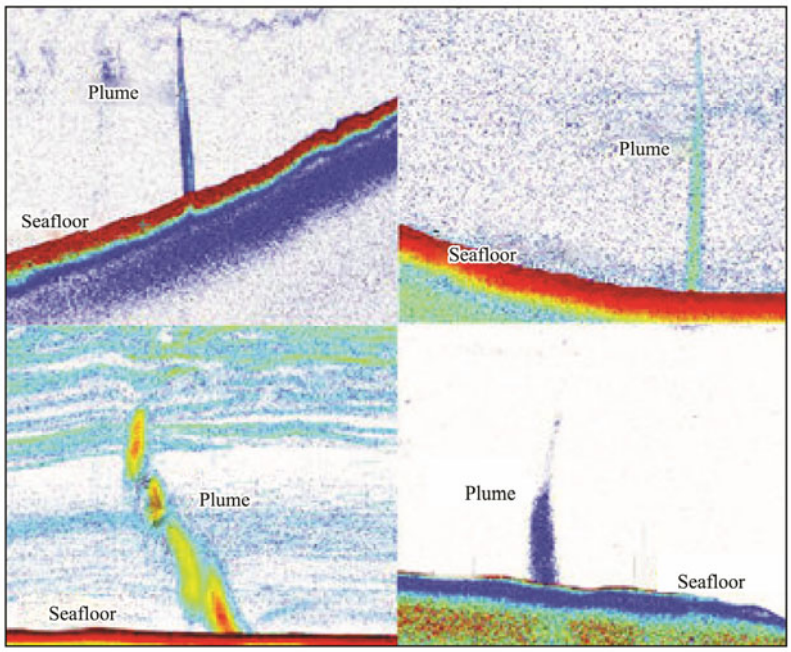

Fig.1 Cold seepages and bubble plumes discharged from the Okhotsk Sea (from Luan *et al.*, 2010).

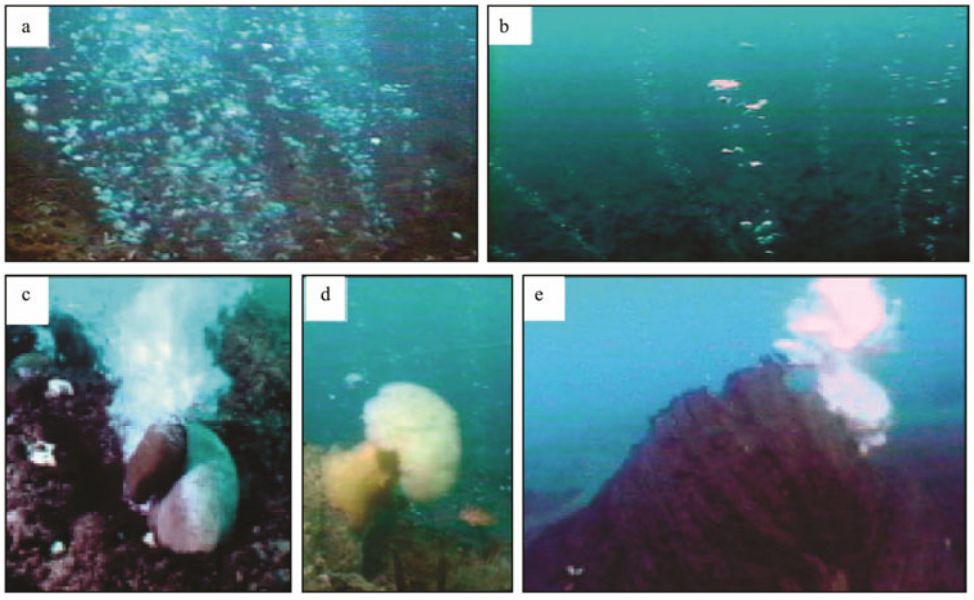

Fig.2 Cold seep bubble plumes in different eruption forms near mud volcano (from Leifer, 2010).

It has been observed that typical seafloor cold seep activity areas in the world have methane seepage in high concentration which can be hundreds to thousands of times the seawater background value (2–5 nmol L^{-1}). For example, the cold seep in the Hikurangi margin in the North Island of New Zealand has a methane concentration of over 500 nmol L^{-1} (Faure *et al.*, 2010). The methane concentration of seawater near the bottom of the Black Sea is 50 nmol L^{-1} to 5.5 μmol L^{-1} (Schmale *et al.*, 2010). The methane concentration in the plume in the Santa Barbara Channel reaches 1600 nmol L^{-1} (Mau *et al.*, 2006). The methane concentration near the bottom of the cold seep exposure area of the northern slope in the South China Sea reaches 3.8 μmol L^{-1} to 4.2 μmol L^{-1}, which is over 300–1000 times the overlying water concentration and seawater background value (Xu, 2013).

The primary research objective of conventional marine seismic exploration technology are seafloor sediments and the geological structure beneath, which usually relegates the information related to seawater as noise when pre-processing marine multichannel seismic data. When Holbrook *et al.* (2003) successfully applied the reflection seismology method in physical oceanography for the first time in 2003, interdisciplinary seismic oceanography expanded to include traditional reflection seismology for application to studing seawater (Liu and Song, 2012). Consequently, researchers started to use the seismic exploration technology to study marine water characteristics (parameters including salinity, temperature, velocity and density) (Hu *et al.*, 2009). Song *et al.* (2008), Chen *et al.* (2011), Dong *et al.* (2010) and Pinheiro *et al.* (2010) carried out further research in this field, achieving some important research results in the offshore continental margin of Iberia, Cadiz Bay, the South China Sea and the adjacent sea areas of Taiwan. Zheng and Yan (2010) used seismic oceanography to study the seawater structure of the northeastern South China Sea and obtain the acoustic velocity profile of seawater and visual images of seawater body structure through processing of the reflection signal of the water body.

At present, the main detection method of a seafloor cold seep includes multi-beam sounding, single-beam sonar, side scan sonar, sub-bottom profiling, seafloor visual observation, geochemical analysis, *etc.* (Liu and Song, 2012). The plumes are usually identified through photography and sonar acoustic technology (Luan and Liu, 2010; Sauter *et al.*, 2006; Shipboard Scientific Party, 2002; Sassen *et al.*, 2001), showing high-resolution images and visible plumes. Since the scale of a plume bubble is much smaller compared to the acoustic wavelength, according to the scattering theory (Wu and Aki, 1993) scattering will occur when the acoustic wave meets the bubble. Therefore, the plumes can be detected by conducting scattering imaging of seawater seismic data. A seismic response generated by the plume can clearly be seen from non-conventional seismic processing of the seismic section of the hydrate in the South China Sea (Li *et al.*, 2013a), which has the cold seep development. Therefore, the seismic method can be used to detect the bubble plume in the water body. Moreover, for regional exploration, the seismic method is one of the major methods to detect plumes. However, a complete system of methods has not been formed regarding the processing of seismic data to identify the plume, and the seismic response mechanism of the plume is unclear.

Citing the above problems, this project seeks to conduct research on numerical simulation of the plume, and build the model of a plume water body through bubble-contained medium acoustic velocity models and stochastic medium theory based on acoustic characteristics of a bubble-contained water body and actual plume characteristics. A single-shot seismic record from forward modelling demonstrates the characteristics of a scattered wave field generated by a plume. The seismic attributes of plume pre-stack shot gather records are extracted to obtain the relationship between the bubble content and the seismic attributes, and we find that the change in bubble content will cause obvious changes in the seismic attributes and the change in bubble radius will not cause changes in the seismic attributes. The above research results can provide a theoretical reference basis for the identification of hydrate plumes with the seismic method, which will benefit the ongoing exploration of hydrate decomposition and migration as well as the distribution of methane bubbles in the seawater, and thus will provide a theoretical reference for the research on the marine environmental changes caused by bubble plumes with the seismic method.

Because this paper is a continued work from the first author's series of papers on this topic as mentioned in the Bibliography (Li *et al.*, 2013b; Li *et al.*, 2016), the model of a bubble plume (Fig.3) and its shot gather seismic record (Fig.4) in this paper are the same as Fig.3 and Fig.4 in Li *et al.* (2016).

2 Model of Bubble Plume Water Body

In the cold seep activity area, the plume phenomenon is caused by bubbles generated by the seepage of methane gas in the seawater, which will change the distribution of pressure in the seawater in addition to changing the acoustic characteristics of the seawater. The acoustic velocity of bubble-contained seawater is related to the bubble radius and the bubble content, and the acoustic velocity of a bubble plume can be obtained by the bubble-contained medium acoustic velocity model (Li *et al.*, 2013b). According to the changes in the bubble radius during its ascent through the seawater (Sauter *et al.*, 2006; Leifer, 2010), the plume is divided into three cycles within the depth range of 1000 m, from shallow to deep: Cycle 1, Cycle 2, and Cycle 3. The longitudinal variation of bubble radius and content in each cycle increases first and then decreases. That is, the bubbles begin to gush or split into small bubbles after rising to a certain height, causing a decrease in the radius, and the content decreases (*i.e.*, the content is the volume content, and it will correspondingly decrease). Because the plume bubbles are distributed in seawater stochastically, and the gas-liquid two-phase medium also belongs to the stochastic medium, the

stochastic disturbance is explained by stochastic medium theory, which makes bubble radius and content at each layer in each cycle change with stochastic variation of background bubble radius and background content (Li *et al.*, 2013b). To avoid repetition, the details of the model setup, such as the grid size, time step, and distribution of the random medium, are referred to Li *et al.* (2016).

The model of a plume water body is built according to the above theory, as shown in Fig.3 (Li *et al.*, 2016). To achieve the imaging result, the homogeneous layer of 250 m is added at the bottom of the model (velocity of 1520 m s^{-1}), equivalent to a seafloor homogeneous layer.

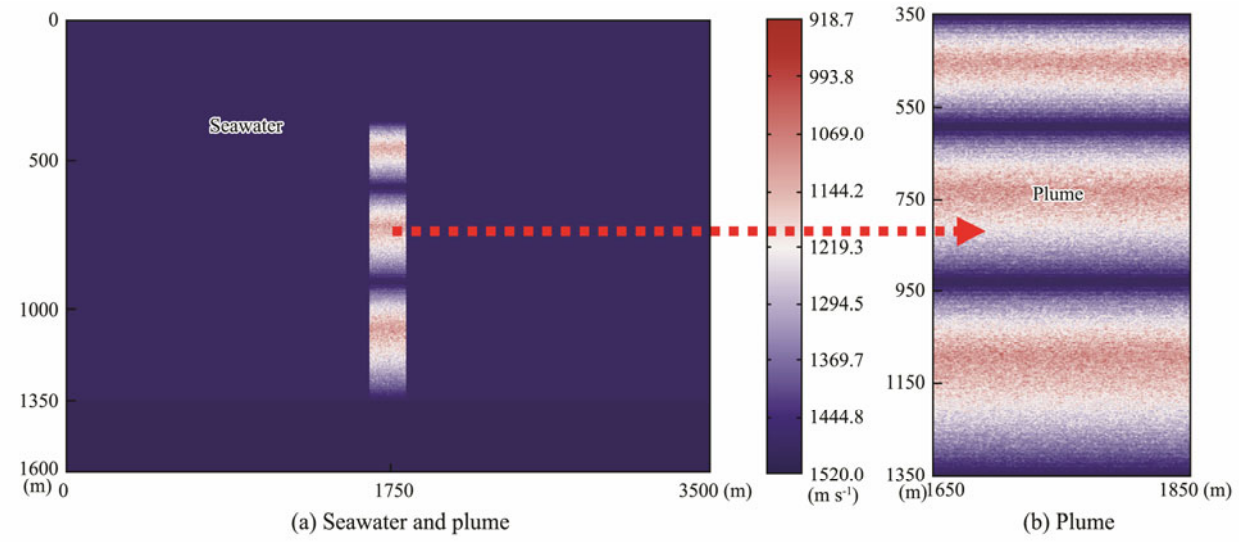

Fig.3 Velocity model of plume water body constructed by bubble-contained medium acoustic velocity model and stochastic medium theory (from Li *et al.*, 2016).

To study the impact of bubble content on seismic response characteristics, six models of the plume water body are built. The variation range of bubble radius in these six models is the same but with different content, which is equivalent to the variation of the number of bubbles. That is, when the bubble content increases (constant radius), the number of bubbles increases, and when the bubble content decreases (constant radius), the number of bubbles decreases. To facilitate the differentiation, the six models are named, respectively, as mod82_1, mod82_2, mod82_3, mod82_4, mod82_5 and mod82_6.

The variation range of the bubble background radius of six models is as follows, respectively.

In the Cycle 1, the bubble background radius ranges from 4.6×10^{-4} m to 4.6×10^{-3} m to 4.6×10^{-4} m.

In the Cycle 2, the bubble background radius ranges from 4.8×10^{-4} m to 4.8×10^{-3} m to 4.8×10^{-4} m.

In the Cycle 3, the bubble background radius ranges from 5.0×10^{-4} m to 5.0×10^{-3} m to 5.0×10^{-4} m.

The bubble content of six models is shown in Table 1.

Table 1 Bubble background content of six models

Model	Bubble background content in cycle 1	Bubble background content in cycle 2	Bubble background content in cycle 3
Mod82_1	$0.8\times10^{-6}-3.6\times10^{-5}-0.8\times10^{-6}$	$0.6\times10^{-6}-3.8\times10^{-5}-0.6\times10^{-6}$	$0.5\times10^{-6}-4.0\times10^{-5}-0.5\times10^{-6}$
Mod82_2	$1.3\times10^{-6}-4.1\times10^{-5}-1.3\times10^{-6}$	$1.1\times10^{-6}-4.3\times10^{-5}-1.1\times10^{-6}$	$1.0\times10^{-6}-4.5\times10^{-5}-1.0\times10^{-6}$
Mod82_3	$1.8\times10^{-6}-4.6\times10^{-5}-1.8\times10^{-6}$	$1.6\times10^{-6}-4.8\times10^{-5}-1.6\times10^{-6}$	$1.5\times10^{-6}-5.0\times10^{-5}-1.5\times10^{-6}$
Mod82_4	$2.3\times10^{-6}-5.1\times10^{-5}-2.3\times10^{-6}$	$2.1\times10^{-6}-5.3\times10^{-5}-2.1\times10^{-6}$	$2.0\times10^{-6}-5.5\times10^{-5}-2.0\times10^{-6}$
Mod82_5	$2.8\times10^{-6}-5.6\times10^{-5}-2.8\times10^{-6}$	$2.6\times10^{-6}-5.8\times10^{-5}-2.6\times10^{-6}$	$2.5\times10^{-6}-6.0\times10^{-5}-2.5\times10^{-6}$
Mod82_6	$3.3\times10^{-6}-6.1\times10^{-5}-3.3\times10^{-6}$	$3.1\times10^{-6}-6.3\times10^{-5}-6.1\times10^{-6}$	$3.0\times10^{-6}-6.5\times10^{-5}-3.0\times10^{-6}$

To study the impact of changes in bubble radius on seismic response characteristics, the following four models of plume water bodies are built. The variation range of bubble content of these four models is the same but with different radius, which is equivalent to the variation in the number of bubbles. That is, when the bubble radius increases (constant content), the number of bubbles decreases, and when the bubble radius decreases (constant content), the number of bubbles increases. To facilitate the differentiation, the four models are named respectively as mod82_7, mod82_8, mod82_9 and mod82_10.

The variation range of the bubble background content of four models is as follows, respectively.

In the Cycle 1, the bubble background content ranges from 3.3×10^{-6} to 6.1×10^{-5} to 3.3×10^{-6}.

In the Cycle 2, the bubble background content ranges from 3.1×10^{-6} to 6.3×10^{-5} to 3.1×10^{-6}.

In the Cycle 3, the bubble background content ranges from 3.0×10^{-6} to 6.5×10^{-5} to 3.0×10^{-6}.

The bubble radius of four models is shown in Table 2.

The specifications in the 10 models above are the same in Fig.3. With different background values of bubble

content and radius, the model diagrams are not listed as follows. Consider that, as the depth of seawater decreases, the pressure decreases, the bubble radius increases, and the content increases. At the same time, as the bubbles divide into smaller bubbles and the number of bubbles changes, the starting and ending values of background radius and background content of each model in the three cycles are different.

Table 2 Bubble background radius of four models

Model	Bubble background radius in cycle 1 (m)	Bubble background radius in cycle 2 (m)	Bubble background radius in cycle 3 (m)
Mod82_7	$0.6\times10^{-4}-0.6\times10^{-3}-0.6\times10^{-4}$	$0.8\times10^{-4}-0.8\times10^{-3}-0.8\times10^{-4}$	$1.0\times10^{-4}-1.0\times10^{-3}-1.0\times10^{-4}$
Mod82_8	$2.6\times10^{-4}-2.6\times10^{-3}-2.6\times10^{-4}$	$2.8\times10^{-4}-2.8\times10^{-3}-2.8\times10^{-4}$	$3.0\times10^{-4}-3.0\times10^{-3}-3.0\times10^{-4}$
Mod82_9	$4.6\times10^{-4}-4.6\times10^{-3}-4.6\times10^{-4}$	$4.8\times10^{-4}-4.8\times10^{-3}-4.8\times10^{-4}$	$5.0\times10^{-4}-5.0\times10^{-3}-5.0\times10^{-4}$
Mod82_10	$6.6\times10^{-4}-6.6\times10^{-3}-6.6\times10^{-4}$	$6.8\times10^{-4}-6.8\times10^{-3}-6.8\times10^{-4}$	$7.0\times10^{-4}-7.0\times10^{-3}-7.0\times10^{-4}$

3 Shot Gather Seismic Record of the Plume

The method of solving the 2D acoustic wave equation with finite difference (Li *et al.*, 2014; Zhang *et al.*, 2014) is used to carry out forward modelling of the above ten models of plume water bodies to obtain their respective shot gather seismic records, from which the shot gather seismic records of the shot points are in the middle position of one model, as shown in Fig.4 (Li *et al.*, 2016). Similarly, in order to avoid repetition, the acquisition parameters of shot gather are referred to Li *et al.* (2016).

In the shot gather record in Fig.4, the seismic wave field of the position of the plume has obvious characteristics of a scattered wave field. In the single-shot seismic record, the scattered wave energy in relation to the centre of the plume is strongest, and the energy gradually decreases on both sides, decreasing faster both upwards and downwards. The energy is stronger at the position with larger and denser concentrations of bubbles. The seismic waveform at the position of the bubbles is reflected as a scattered wave series with the position of bubbles as the peak, and coherence increases at the position of relatively high bubble distribution density. The minimum value of relatively strong scattered wave energy during travelling is always located immediately above the plume, which is not related to the position of the shot point. The shot gather record (Fig.4) displays the cycle characteristics of the models (Fig.3). In particular, the plume is more obvious at the middle position of the shot gather record, and the energy in three cycles gradually decreases from up to down.

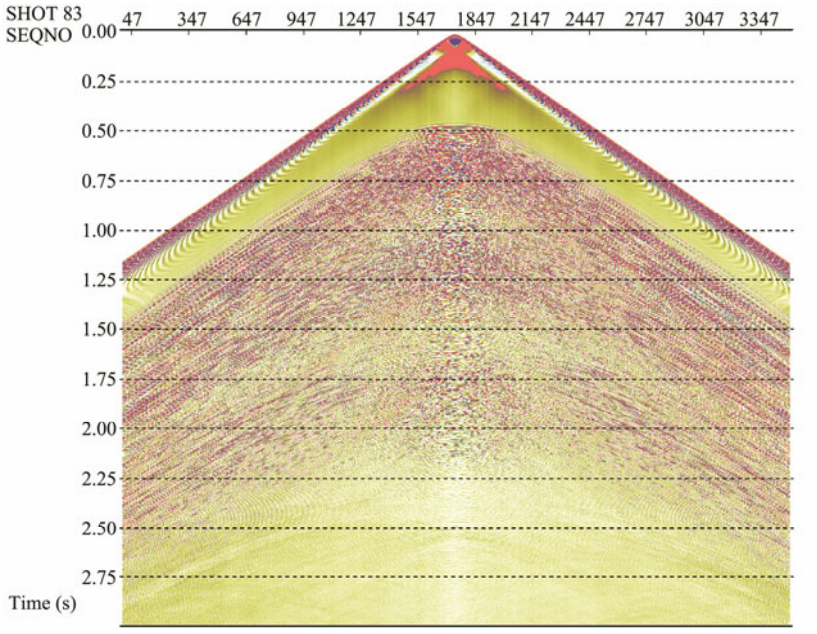

Fig.4 The 83th shot gather seismic record of plume model corresponding to Fig.3 (From Li *et al.*, 2016).

4 Extracted Seismic Attributes

The research on seismic attributes began in the late 1970s, developed rapidly in the late 1980s, and became mature after the 1990s (Cao, 2004; Xu *et al.*, 2010). The characteristics of seismic attributes are special values related to characteristics of geometry, kinematics, dynamics and statistics extracted from the seismic data, and different attributes have different effects based upon different geological environment and different detection goals. According to the classification of seismic attributes based on the kinematics and dynamics of seismic waves as well as reservoir characteristics (Zhuang, 1999; Qi and

Zhang, 2012), this paper extracted the following six seismic attributes (Zou and Zhang, 2002).

RMS Amplitude, which is used to calculate the RMS of seismic record samples within the starting and ending time in the chosen time window, is calculated with the formula

$$att1 = \sqrt{\frac{1}{n_2 - n_1}\sum_{n=n_1}^{n=n_2} A^2(n\cdot\Delta t)}\ . \tag{1}$$

The Average Absolute Amplitude is calculated with the formula

$$att2 = \frac{\sum_{n=n_1}^{n=n_2} \left|A(n\cdot\Delta t)\right|}{n_2 - n_1}. \tag{2}$$

Average Energy Variation, which is the average energy of all sampling points in the chosen time window (amplitude square), is calculated using the formula

$$att3 = \frac{\sum_{n=n_1}^{n=n_2} A^2(n\cdot\Delta t)}{n_2 - n_1}. \tag{3}$$

Kurtosis in Amplitude is the sum of the fourth power of the amplitude of all sampling points in the chosen time window, and is the measure of the relative swing of the amplitude. The calculation formula is:

$$att4 = \sum_{n=n_1}^{n=n_2} A^4(n\cdot\Delta t). \tag{4}$$

Absolute Amplitude Integral is the sum of the amplitude absolute of amplitude of all sampling points in the chosen time window. This sum's calculation formula is

$$att5 = \sum_{n=n_1}^{n=n_2} \left|A(n\cdot\Delta t)\right|. \tag{5}$$

We also obtain the amplitude in the frequency domain $X(n)$ through a Fast Fourier Transform, and extract the total energy attribute (*i.e.*, the square sum of the amplitude), which is related to factors such as the reflection coefficient of the stratum. In the oil and gas-bearing range, the total energy of the waveform usually has a strong response. The calculation formula in the chosen time window is:

$$att6 = S = \sum_{n=1}^{N} X^2(n). \tag{6}$$

In Formulas (1), (2), (3), (4) and (5), Δt is the sampling interval; n_1, n_2 are the sampling points, respectively, corresponding to the top and bottom of the time window; n_2-n_1 is the number of sampling points in time window; $A(n\cdot\Delta t)$ is the instantaneous amplitude; $|A(n\cdot\Delta t)|$ is the absolute instantaneous amplitude; $X(n)$ is the amplitude of the n sampling points in the frequency domain; *attm* is the *m* extracted attribute.

5 Research on Relationship Between Model Parameters and Seismic Attributes

The seismic attributes are extracted from the shot gather seismic record of each plume model to study the impact of changes in bubble content and bubble radius on seismic attributes.

5.1 Extraction Method of Seismic Data

We select the seismic data from Channel 1701 to Channel 1800 (100 channels in total) in the 83rd shot gather seismic record of ten plume models, and extract the data longitudinally from the positions in three cycles in the model, respectively. There are 350 sampling points in total from Sampling Point 501 to Sampling Point 850 in Cycle 1; there are 450 sampling points in total from Sampling Point 901 to Sampling Point 1350 in Cycle 2; there are 600 sampling points in total from Sampling Point 1501 to Sampling Point 2100 in Cycle 3. Thus, the single shot seismic data for the calculation of seismic attributes is a rectangular 2D data volume, 350 lines by 100 columns in Cycle 1, 450 lines by 100 columns in Cycle 2, and 600 lines by 100 columns in Cycle 3. The seismic attributes are, respectively, extracted according to the bubble content (corresponding to the former six models) and bubble radius (corresponding to the latter four models).

5.2 Relationship Between Seismic Attributes and Bubble Content

Through the above data extraction method, the seismic data of the former six models are extracted. According to the calculation formulas (Formulas (1) to (6)) of six attributes, the seismic attributes of each model (corresponding to different bubble content) are calculated, and the bubble content and the extracted seismic attributes are displayed as a 2D linear graph, as shown in Fig.5. To better display the variation trend of seismic attributes against the variation of bubble content, a trend line (dotted line in Fig.5) is added based on the original linear graph. Thus, the diagram of correlation between the bubble content and the seismic attributes is obtained.

Because the diagrams of relationships between Average Energy Variation, RMS Amplitude, Average Absolute Amplitude and bubble content are similar, only the diagram of relationship between Average Absolute Amplitude and bubble content is listed.

The following points can be obtained from Fig.5.

First, the change in bubble content will cause a change in seismic attributes. That is, the change in plume bubble content will cause a change in the seismic response on the seismic section, which can be explained by the previous research results (Li *et al.*, 2010). The change in bubble content will cause a change in acoustic velocity, thus causing a change in seismic response.

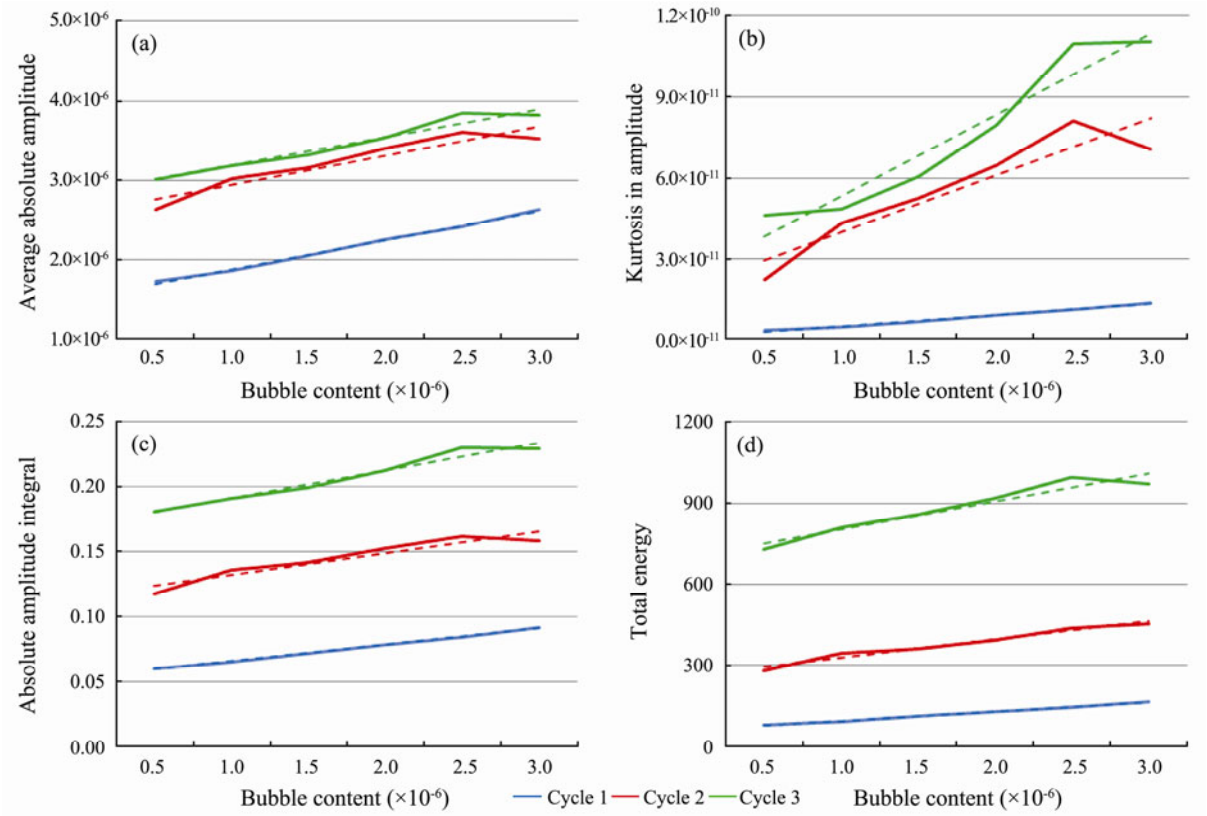

Fig.5 Relationship between bubble content and seismic attributes in shot gather record of the plume.

Second, the relationship between bubble content and seismic attributes can be obtained. That is, with an increase in bubble content, the attribute value of seismic amplitude increases, and they are positively correlated. In addition, the variation laws of attributes in three cycles are consistent, which is because the bubble radius increases with an increase in bubble content (the bubble content is the volume content). When the scattering surface of the seismic wave scattering increases, the energy of scattered wave will increase, which is consistent with the characteristics in the shot gather seismic record in Fig.4. That is, the energy is stronger when the bubbles are larger and more numerous, and the seismic waveform at the position of the bubbles is reflected as a scattered wave series with the position of bubbles as the peak, and coherence increases at the position of relatively high bubble distribution density.

Third, for certain content, the variation laws in the three cycles are that the attribute value in Cycle 1, Cycle 2 and Cycle 3 increases, in turn, because the variation range of bubble content set in the model increases in turn, which causes an increase in amplitude energy in turn. In addition, the data in three cycles for the extraction of seismic data increases in turn, and the attribute value related to the amplitude is sure to increase in turn.

5.3 Relationship Between Seismic Attributes and Bubble Radius

Through the data extraction method, the seismic data of the latter four models are extracted. According to the calculation formulas of the six attributes, the seismic attributes of each model (corresponding to different bubble radius) are calculated, and the bubble radius and the extracted seismic attributes are displayed as a 2D linear graph, as shown in Fig.6.

Because seismic attributes of shot gather seismic records are seldom affected by the bubble radius, and the diagrams of the relationship between the six attributes and bubble radius are similar, only the Average Absolute Amplitude, Absolute Amplitude Integral, and Total Energy are listed here.

The following points can be obtained from Fig.6.

First, when the bubble radius changes, the seismic attributes do not change significantly. That is, when the bubble radius of the plume changes, the change in seismic response caused on the seismic section is small, which can be explained by previous research (Li *et al.*, 2010). That is, the impact of change in bubble radius on the acoustic velocity is relatively small, thus causing little change in seismic response.

Second, for certain content, the variation laws in three cycles are the same as that of bubble content. The attribute values in Cycle 1, Cycle 2 and Cycle 3 increase in turn, which is observed primarily because the data in the three cycles for the extraction of seismic data increases in turn, and the attribute value related to the amplitude is sure to increase in turn.

6 Conclusions

This paper built the model of a plume water body through bubble-contained medium acoustic velocity mod-

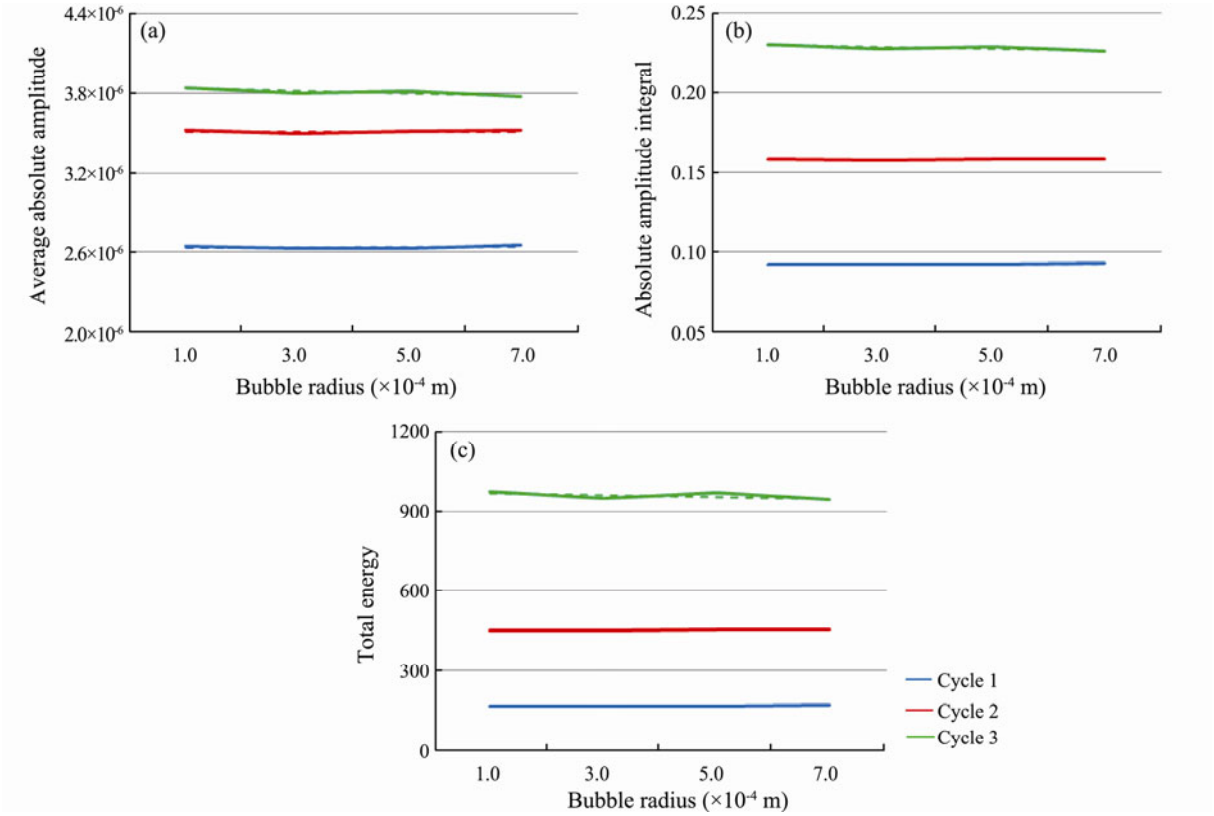

Fig.6 Relationship between bubble radius and seismic attributes in shot gather record of the plume.

els and stochastic medium theory. The finite difference method is used for forward modelling of the model, and the single-shot seismic record shows the characteristics of a scattered wave field generated by plume. To study the impact of bubble content and bubble radius on the seismic response characteristics, ten models of a plume water body are built to carry out forward modelling and obtain the shot gather seismic record. The relationship between the bubble radius and bubble content of model parameters and the seismic attributes is studied through the seismic attributes extracted from pre-stack shot gather seismic record of ten plume models.

Through the above research, the following conclusions are reached as follows.

First, the analysis of characteristics of the scattered wave field of the plume provides a theoretical reference for the identification of bubble plumes with scattered waves.

Second, the change in bubble content of the plume will cause obvious changes in the seismic response, and a positive correlation exists between pre-stack shot gatherseismic attributes and bubble content of the model parameters. When the bubble content increases, the seismic attribute value increases.

Third, the change in bubble radius of the plume will not cause the change in seismic response, and an obvious independence exists between pre-stack shot gather seismic attributes and bubble radius.

The above research on seismic attributes of the plume is preliminary, and the research on this topic will continue regarding the seismic attributes of stacked sections of the plume. Because the plume is closely related to the distribution of methane bubbles in seawater and the existence of cold seeps and natural gas hydrate, this research can provide a theoretical basis for the identification of natural gas hydrate, which will benefit the further exploration of hydrate decomposition and migration as well as the distribution of methane bubbles in the seawater. This study will provide a theoretical reference for research on marine environmental changes caused by bubble plume utilizing the seismic method. Therefore, the methane plume in the seawater is the subject worth further study.

Acknowledgements

This study was financially supported by the National Natural Science Foundation of China (No. 41306050), the Science and Technology Project of Guangdong Province of China (No. 2014A010103030), the Natural Science Foundation of Guangdong Province under contract (No. 2015A030313617) and the National Marine Important Charity Special Foundation of China (No. 201305019).

References

Bayon, G., Birot, D., and Ruffine, L., 2011. Evidence for intense REE scavenging at cold seeps from the Niger Delta margin. *Earth and Planetary Science Letters*, **312** (3): 443-452.

Cao, H., 2004. Discussion on several key problems in the application of seismic attributes. *Geophysical Prospecting for Petroleum*, **43** (S): 1-3.

Charloua, J. L., Donvala, J. P., and Zitterd, T., 2003. Evidence of methane venting and geochemistry of brines on mud volca-

noes of the eastern Mediterranean Sea. *Deep-Sea Research I: Oceanographic Research Papers*, **50** (8): 941-958.

Chen, D. F., and Cathles, L. M., 2005. On the thermal impact of gas venting and hydrate crystallization. *Journal of Geophysics Research: Solid Earth*, **110** (B11): 5391-5392.

Chen, D. F., Li, X. X., and Xia, B., 2004. Distribution of gas hydrate stable zones and resource prediction in the Qiongdongnan Basin of the South China Sea. *Chinese Journal of Geophysics*, **47** (3): 483-489 (in Chinese with English abstract).

Chen, D. F., Liu, Q., Zhang, Z, W., Cathles III, L. M., and Roberts, H. H., 2007. Biogenic fabrics in seep carbonates from an active gas vent site in Green Canyon Block 238, Gulf of Mexico. *Marine and Petroleum Geology*, **24** (5): 313-320.

Chen, J. X., Song, H. B., Huang, X. H., and Bai, Y., 2011. The development prospect and the progress on seismic oceanography. *China Geophysical Society 27th Annual Meeting*. Changsha, 915 (in Chinese with English abstract).

Chen, Z., Yan, W., and Chen, M. H., 2006. Discovery of seep carbonate nodules as new evidence for gas venting on the northern continental slope of South China Sea. *Chinese Science Bulletin*, **51** (10): 1228-1237.

Di, P. F., Feng, D., Gau, L. B., and Chen, D. F., 2008. *In situ* measurement of fluid flow and signatures of seep activity at marine seep sites. *Progress in Geophysics*, **23** (5): 1592-1602 (in Chinese).

Di, P. F., Huang, H. G., and Chen, D. F., 2010. Total sulfur and calcium contents of seep fluids and their controls in the cold seep sites. *Geoscience*, **24** (3): 570-575, 580 (in Chinese with English abstract).

Dong, C. Z., Song, H. B., Bai, Y., Huang, X. H., and Song, Y., 2010. The progress on seismic oceanography. *Progress in Geophysics*, **25** (1): 109-123.

Faure, K., Greinert, J., and Deimling, J. V., 2010. Methane seepage along the Hikuran-gi Margin of New Zealand: geochemical and physical data from the water column, sea surface and atmosphere. *Marine Geology*, **272** (1-4): 170-188.

Feng, D., Chen, D. F., and Peckmann, J., 2009a. Rare earth elements in seep carbonates as tracers of variable redox conditions at ancient hydrocarbon seeps. *Terra Nova*, **21** (1): 49-56.

Feng, D., Chen, D. F., and Roberts, H. H., 2009b. Petrographic and geochemical characterization of seep carbonate from Bush Hill (GC 185) gas vent and hydrate site of the Gulf of Mexico. *Marine and Petroleum Geology*, **26** (7): 1190-1198.

Freire, A. F. M., Matsumoto, R., and Santos, L. A., 2011. Structural-stratigraphic control on the Umitaka Spur gas hydrates of Joetsu Basin in the eastern margin of Japan Sea. *Marine and Petroleum Geology*, **28** (10): 1967-1978.

Gong, J. M., 2006. Methane plumes on marine gas hydrate ore reservoir in the east edge of Japan Sea–The possible mechanism of ground methane transporting to the shallow water. *Marine Geology Letters*, **22** (5): 33 (in Chinese).

Greinert, J., Artemov, Y., and Egorov, V, De Batist, M., and McGinnis, D., 2006. 1300-m-high rising bubbles from mud volcanoes at 2080 m in the Black Sea–Hydroacoustic characteristics and temporal variability. *Earth and Planetary Science Letters*, **244** (1-2): 1-15.

Hu, Y., Liu, H. S., and Chen, J., and Xu, J., 2009. Recent progress in seismic oceanography. *Advances in Earth Science*, **24** (10): 1094-1104.

Huang, Y. Y., Sues, S. E., and Wu, N. Y., 2005. The geological background and the evidence of the existence of the natural gas hydrate at Northeast in Dongsha sea area. *Cross Strait Symposium on Natural Gas Hydrate*, Taiwan, 3-4.

Huang, Y. Y., Sues, S. E., and Wu, N. Y., 2008. *The Methane and Natural Gas Hydrate Geology in Northern Slope of the South China Sea*. Geological Publishing House, Beijing, 100-150.

Holbrook, W. S., Paramo, P., and Pearse, S., and Schmitt, R. W., 2003. Thermohaline fine structure in an oceanographic front from seismic reflection profiling. *Science*, **301** (5634): 821-824.

Klaucke, I., Weinrebe, W., and Petersen, C. J., 2010. Temporal variability of gas seeps offshore New Zealand: Multi-frequency eoacoustic imaging of the Wairarapa area, Hikurangi margin. *Marine Geology*, **272** (1-4): 49-58.

Leifer, I., 2010. Characteristics and scaling of bubble plumes from marine hydrocarbon seepage in the Coal Oil Point seep field. *Journal of Geophysical Research: Oceans*, **115**: C11.

Li, C. P., Gou, L. M., and You, J. C., Liu, X. W., and Ou, C. L., 2016. Further studies on the numerical simulation of bubble plumes in the cold seepage active region. *Acta Oceanologica Sinica*, **35** (1): 118-124.

Li, C. P., Liu, X. W., and Zhao, L. C., 2013a. Progress on cold seeps and bubble plumes produced by gas hydrate. *Progress in Geophysics*, **28** (2): 1048-1056 (in Chinese with English abstract).

Li, C. P., Liu, X. W., Gou, L. M., and Wang, X. C., 2013b. Numerical simulation of bubble plumes in overlying water of gas hydrate in the cold seepage active region. *Science China: Earth Sciences*, **56** (4): 579-587.

Li, C. P., Liu, X. W., Yang, L., Jing, H. E., and Lu, L. X., 2010. Study on the bubble radius and content effect on the acoustic velocity of seawater with bubbles. *Geoscience*, **24** (3): 528-533.

Li, T. C., Xie, Y. H., Li, L., Wang, H. Z., Wang, X. L., and Dan, Z. W., 2014. Visco-acoustic medium plane-wave finite-difference pre-stack depth migration and its application in Yinggehai Basin. *Chinese Journal of Geophysics*, **57** (5): 1612-1622 (in Chinese with English abstract).

Liu, B. R., and Song, H. B., 2012. Detection of seabed seep by seismic oceanography. *China Geophysical Society 28th Annual Meeting*. Beijing, 730 (in Chinese with English abstract).

Luan, X. W., Liu, H., and Yue, B. J., 2010. Characteristics of cold seepage on side scan sonar sonogram. *Geoscience*, **24** (3): 474-480 (in Chinese with English abstract).

Macdonalda, I. R., Bender, L. C., Vardaro, M., Bernard, B., and Brooks, J. M., 2005. Thermal and visual time series at a seafloor gas hydrate deposit on the Gulf of Mexico slope. *Earth and Planetary Science Letters*, **233** (122): 45-59.

Mau, S., Sahling, H., and Rehder, G., Suess, E., Linke, P., and Soeding, E., 2006. Estimates of methane output from mud extrusions at the erosive convergent margin off Costa Rica. *Marine Geology*, **225** (1-4): 129-144.

Pinheiro, L. M., Song, H. B., and Ruddick, B., Dubert, J., Ambar, I., Mustafa, K., and Bezerra, R., 2010. Detailed 2-D imaging of the Mediterranean outflow and meddies off W Iberia from multichannel seismic data. *Journal of Marine Systems*, **79** (1-2): 89-100.

Qi, X. M., and Zhang, S. C., 2012. Application of seismic multi-attribute fusion method based on D-S evidence theory in prediction of CBM-enriched area. *Applied Geophysics*, **9** (1): 80-86.

Sassen, R., Losh, S. L., and Cathles III, L., Roberts, H. H., Whelan, J. K., Milkov, A. V., Sweet, S. T., and DeFreitas, D. A., 2001. Massive vein-filling gas hydrate: Relation to ongoing gas migration from the deep subsurface in the Gulf of Mexico. *Marine and Petroleum Geology*, **18** (5): 551-560.

Sauter, E. J., Muyakshin, S. I., Charlou, J.-L., Schlüter, M., Boetius, A., Jerosch, K., Damm, E., Foucher, J.-P., and Klages, M., 2006. Methane discharge from a deep-sea submarine mud volcano into the upper water column by gas hydrate-coated methane bubbles. *Earth and Planetary Science Letters*, **243** (3-4): 354-365.

Schmale, O., Beaubien, S. E., and Rehder, G., Greinert, J., and Lombardi, S., 2010. Gas seepage in the Dnepr paleo-delta area (NW-Black Sea) and its regional impact on the water column methanecycle. *Journal of Marine Systems*, **80** (1-2): 90-100.

Shipboard Scientific Party, 2002. *Ocean Drilling Program Leg 204 Preliminary Report*. Texas A&M University, December 2002, USA.

Song, H. B., Dong, C. Z., and Chen, L., and Song, Y., 2008. Reflection seismic methods for studying physical oceanography: Introduction of seismic oceanography. *Progress in Geophysics*, **23** (4): 1156-1164 (in Chinese with English abstract).

Tong, H. P., and Chen, D. F., 2012. First discovery and characterizations of late Cretaceous seep carbonates from Xigaze in Tibet, China. *Chinese Science Bulletin*, **57** (33): 4363-4372.

Tryon, M. D., and Brown, K. M., 2004. Fluid and chemical cycling at Bush Hill: Implications for gas and hydrate-rich environments. *Geochemistry, Geophysics, Geosystems*, **5** (12): 1-7.

Tryon, M. D., Brown, K. M., and Torres, M. E., 2002. Fluid and chemical flux in and out of sediment s hosting methane hydrate deposits on Hydrate Ridge, OR, II: Hydrological processes. *Earth and Planetary Science Letters*, **201** (324): 541-557.

Wu, R. S., and Aki, K., 1989. *Scattering and Attenuation of Seismic Waves, Part II*. Springer Basel AG, 191pp.

Xu, C. L., 2013. In situ observation of Methane seepage in the South China Sea. Master thesis. Ocean University of China, Qingdao.

Xu, H. N., Yang, S. X., Zheng, X. D., Wang, M. J., and Wang, J. S., 2010. Seismic identification of gas hydrate and its distribution in Shenhu Area, South China Sea. *Chinese Journal of Geophysics*, **53** (7): 1691-1698 (in Chinese with English abstract).

Ye, L. M., Luo, P., and Yang, K. H., 2011. Advances in climatic effects study of gas hydrates. *Advances in Earth Science*, **26** (5): 565-574 (in Chinese with English abstract).

Zhang, H., Liu, H., Liu, L., Jin, W. J., and Shi, X. D., 2014. Frequency domain acoustic equation high-order modeling based on an average-derivative method. *Chinese Journal of Geophysics*, **57** (5): 1599-1611 (in Chinese with English abstract).

Zhang, Y., Zhang, S. L., and Xue, B. S., 2013. The research progress on exploration of gas hydrate and its main problems. *China Geophysical Society 29th Annual Meeting*. Kunming, 965 (in Chinese with English abstract).

Zheng, H. B., and Yan, P., 2010. The application of seismic oceanography to studying ocean water mass structure in the northeastern South China Sea. *Chinese Journal of Geophysics*, **53** (8): 1852-1858 (in Chinese with English abstract).

Zhuang, D. H., 1999. Research and application of seismic attribute technology and 4D seismic method. PhD thesis. China University of Geosciences, Beijing.

Zou, C. M., and Zhang, Y., 2002. *Practical New Technology of Oil and Gas Exploration and Development*. Petroleum Industry Press, Beijing, 15-25.

(Edited by Xie Jun)